

# Prospects of using MOF/TiO<sub>2</sub> nanocomposites for photocatalytic degradation of pesticides

Zhou Zhentao<sup>1,2</sup>, A. Sukhoivanenko<sup>1</sup>,  
T. Dontsova<sup>1</sup>

<sup>1</sup>National Technical University of Ukraine “Igor Sikorsky Kyiv Polytechnic Institute”, Kyiv 03056, Ukraine

<sup>2</sup>State Key Laboratory for Biology of Plant Disease and Insect Pests, Institute of Plant protection, Chinese Academy of Agriculture Science, Beijing 100193, China

*Received May 25, 2024*

Cleaning water bodies from fourth-generation pesticides is an urgent problem today. In this study, a series of nanocomposites based on MOF (NH<sub>2</sub>-MIL-125) and commercial titanium (IV) oxide P25 were synthesized and characterized, and their photocatalytic activity towards imidacloprid was determined. MOF and MOF/TiO<sub>2</sub> composites were synthesized by a simple solvothermal method. The synthesized MOF and MOF/TiO<sub>2</sub> composite were characterized by XRD, electron microscopy, UV-visible, infrared and FTIR spectroscopy, and TGA analysis. The studies showed that TiO<sub>2</sub> and MOF have typical properties, and the properties of the composite were similar to those of MOF. The found band gap values of MOF and MOF/TiO<sub>2</sub> composite (2.68 eV and 2.58 eV) indicate their potential use visible light photocatalytic processes. The photocatalytic activity study indicates a two-step degradation of imidacloprid, which is quite efficient for the MOF/TiO<sub>2</sub> composite with the highest titanium (IV) oxide content, reaching almost 100% after 2 hour of photocatalytic reaction.

**Keywords:** MOF/TiO<sub>2</sub> nanocomposites, Metal-organic frameworks, Titanium (IV) oxide, Photocatalysis, Pesticides, Imidacloprid

**Перспективність використання нанокompозитів MOF/TiO<sub>2</sub> для фотокаталітичної деградації пестицидів.** Чжоу Чжентао, А. Сухоіваненко, Т. Донцова

Видалення пестицидів четвертого покоління з водних об'єктів є актуальною проблемою сьогодення. В роботі було синтезовано та охарактеризовано серію нанокompозитів на основі MOF (NH<sub>2</sub>-MIL-125) і комерційного титан (IV) оксиду P25 та визначено їх фотокаталітичну активність по відношенню до імідаклоприду. MOF (NH<sub>2</sub>-MIL-125) та композити були синтезовані простим сольвотермальним методом та охарактеризовані методами рентгенофазового аналізу, електронної мікроскопії, УФ-, ІЧ- та Фур'є-спектроскопії, а також методом термічного аналізу. Дослідження показали, що TiO<sub>2</sub> і MOF мають типові для них властивості, а характеристики нанокompозитів були подібні до властивостей MOF. Знайдені значення ширини забороненої зони MOF і обраного нанокompозиту MOF/TiO<sub>2</sub> (2,68 eV і 2,58 eV) вказують на їх потенційне використання у фотокаталітичних процесах у видимому світлі. Дослідження фотокаталітичної активності вказує на двостадійну деградацію імідаклоприду, яка є досить ефективною для нанокompозиту MOF/TiO<sub>2</sub> з найвищим вмістом титан (IV) оксиду, що досягає майже 100% після 2 годин фотокаталітичної реакції.

## 1. Introduction

Neonicotinoids, particularly imidacloprid, are fourth-generation pesticides that have re-

placed organophosphates, pyrethroids and carbamates, and are widely used to control insect pests on various industrial crops. Neo-

nicotinoids are considered ideal replacements for highly toxic pesticides. Numerous studies have reported that neonicotinoids have adverse effects on non-target organisms such as bees, aquatic animals, birds and mammals [1]. As a result, the remediation of neonicotinoid-contaminated environments has gradually become a matter of concern. In particular, imidacloprid can form 6-chloronicotinic acid by oxidative cleavage of guanidine residues, which is ultimately converted to non-toxic carbon dioxide. This raises questions about the non-toxicity of neonicotinoids and their microbial degradation [2].

The most popular methods for removing pesticides from aqueous solutions are adsorption [3], including the use of nanoadsorbents [4], electrocatalytic oxidation [5], sonochemistry [6], membrane technologies [7,8], and photocatalysis [9].

Adsorption of pesticides onto inexpensive materials can effectively treat contaminated water. Nanoparticle-based adsorbents and carbon-based adsorbents have been shown to be highly effective in removing pesticides from water bodies. Electrocatalytic oxidation is a promising and effective approach to remediate pesticide-contaminated environments. Sonochemistry can be an effective method for degrading pesticides in aqueous solutions. Membrane filtration technology is recognized as a promising approach to water and wastewater treatment that can be applied to a wide range of organic micropollutants, including pesticides. Nanofiltration, reverse osmosis and forward osmosis are increasingly being investigated for the removal of pesticides from aquatic environments due to their versatility and high treatment efficiencies.

Advanced oxidation processes (AOPs) are powerful technologies currently used in the treatment of wastewater to decompose organic pollutants, including diverse pesticides [10]. The most widely used AOPs are the Fenton process, heterogeneous photocatalysis, ozonation, electrochemical oxidation, and others. These processes produce highly reactive particles, such as hydroxyl radicals ( $\cdot\text{OH}$ ), ozone molecules ( $\text{O}_3$ ), superoxide radicals ( $\text{O}_2^{\cdot-}$ ), hydrogen peroxide molecules ( $\text{H}_2\text{O}_2$ ), etc.

After the Fenton process, heterogeneous photocatalysis is the second most widely used AOPs [11]. This technology has numerous advantages over other types of AOPs, mainly due to its simplicity and stability. In heteroge-

neous photocatalysis, various semiconductor materials are used as photocatalysts, such as metal oxides ( $\text{TiO}_2$ ,  $\text{SnO}_2$ ,  $\text{Fe}_2\text{O}_3$ ,  $\text{WO}_3$ ,  $\text{ZnO}$ ,  $\text{Ag}_3\text{O}_4$  [12]), metal sulfides ( $\text{ZnS}$ ,  $\text{CdS}$  [13]), and g- $\text{C}_3\text{N}_4$ -based materials [14].

$\text{TiO}_2$  is the most used photocatalyst due to its exceptional properties. These include high physical and chemical stability, high photocatalytic activity, non-toxicity, wide distribution in nature, and low cost [15]. Furthermore, the utilization of  $\text{TiO}_2$  in the form of nanostructures, which have enhanced surface chemistry and increased surface area, is preferred [16]. This results in a quicker and more effective mineralization of organic pollutants.

Although  $\text{TiO}_2$  has a high photocatalytic activity, its wide practical application is limited due to the disadvantage of unfavorable dynamics of photogenerated charge carriers (rapid recombination of electrons and holes in the volume and on the surface of the photocatalyst) [17, 18]. To prevent the recombination of electrons and holes, it is necessary to take certain measures, such as enhancing the separation of charge carriers, prolonging their lifetime, narrowing the width of the photocatalyst band gap, and increasing the surface area of  $\text{TiO}_2$  [19]. Modification of  $\text{TiO}_2$  surface using various strategies [11] can help to achieve these goals. The main methods include doping with metals and nonmetals [20], codoping with metals and nonmetals [13], combining with other semiconductors [21], creating heterojunctions [13] and Z-schemes [22], dye sensitization [13], and creating nanocomposites with Metal-Organic Frameworks (MOFs) [23].

MOFs are porous materials with periodic network structures constructed through the self-assembly of organic ligands with metal nodes connected by coordination bonds [24]. MOFs possess large specific surface areas and are similar to zeolites and inorganic porous molecular sieves. However, MOFs are unique in that they are composed of a wide array of metal nodes and organic ligands with diverse structures and coordination modes.

Compared to conventional porous materials, MOFs offer the benefits of rich structure, chemical functionality, ultra-high specific surface area, and dimensionally tunable morphology [25]. Additionally, MOFs exhibit higher activity and selectivity for organic reactions due to the periodic arrangement of metal nodes and organic ligands in their pore channels, which distinguishes them from inorganic porous zeo-

lites or molecular sieves. Therefore, MOFs are a popular research topic for gas adsorption, storage, separation, and slow drug release [26].

Due to their unique structure, MOFs possess photochemical properties comparable to those of conventional semiconductors like TiO<sub>2</sub> and ZnO. When exposed to light, MOF electrons are transferred from HOMO (highest occupied molecular orbital) to LUMO (lowest unoccupied molecular orbital) orbitals [27], which makes MOF materials photosensitive. Therefore, MOF materials are highly promising for researching applications in the field of photocatalysis [28].

The composition of MOFs typically comprises metal nodes, either metal ions or clusters, and organic ligands. Due to the variety and abundance of the metal nodes and organic ligands that compose MOFs, they are readily functionalized. Therefore, altering the synthesis conditions allows for obtaining distinct morphological structures and specific functionalities of MOF materials by changing the geometric configuration of the secondary structural units, the shape, or the size of the organic ligands. Thus, the wide-ranging physicochemical properties of MOFs determine their applications in different fields [29].

Most of the contemporary techniques for synthesizing metal-organic frameworks involve solvothermal methods. In a few instances, microwave, ultrasound, and electrochemical procedures have also been reported [30,31]. However, most MOFs are very sensitive to water; especially those that retain structural stability in acidic or alkaline environments are very rare [32]. Only a small amount of literature has reported stable MOF materials that can withstand a wide range of pH levels as well as acidic or alkaline solutions [33]. MOFs are often structurally disrupted in humid environments due to the reactivity of their metal nodes. The metal centers, acting as electrophilic reagents, bond with oxygen (nucleophilic reagents) from water molecules in the environment, ultimately destroying the MOF crystal structure. Therefore, the strength of the coordination bonds between the metallic nodes and organic ligands is a critical factor determining the aqueous stability of MOF materials. [34, 35].

In this study, a series of nanocomposites based on MOF (NH<sub>2</sub>-MIL-125) and commercial titanium (IV) oxide P25 were synthesized and characterized, and their photocatalytic activity towards imidacloprid was determined.

## 2. Experimental

### 2.1 Materials

For the synthesis of materials, the following reagents were used: commercial titanium dioxide P25 (containing 80% anatase and 20% rutile), imidacloprid (IMD, 98%) obtained from Aladdin Chemistry Co., Ltd.; 2-aminoterephthalic acid (NH<sub>2</sub>-BDC, AR), titanium isopropoxide (AR), methanol (AR) and N,N-dimethylformamide (DMF, AR) purchased from Macklin Chemistry Co., Ltd.

### 2.2 Synthesis procedures

NH<sub>2</sub>-MIL-125/TiO<sub>2</sub> composites were synthesized by the solvothermal method. Typically, a certain amount of P25 nanoparticles were dispersed into a mixed solution containing 36 mL of DMF and 4 mL of methanol by ultrasonic stirring for 30 min. Then 0.56 g of NH<sub>2</sub>-BDC (3.1 mmol) and 0.6 mL of (2 mmol) were added to the above solution and stirred until the NH<sub>2</sub>-BDC was completely dissolved. Then the mixture was transferred to a 100 mL Teflon-lined stainless-steel autoclave at 150 °C for 24 h. After cooling to room temperature, the solid product was separated by centrifugation and washed several times with DMF and methanol, and dried overnight in a vacuum drying oven at 80°C. The amount of P25 added was calculated by the molar ratio of P25 and precursor, with the ratios of 0.35:1, 1:1, 1.5:1 and 2:1, respectively.

### 2.3. Material characterization

The crystal structure of the samples was examined by X-ray diffraction (XRD, Bruker D8 Advance, Cu K $\alpha$  radiation,  $\lambda = 1.540598 \text{ \AA}$ ). The samples were analyzed over a  $2\theta$  range from 5° to 80°. The morphological and structural images of the samples were obtained by scanning electron microscopy (SEM, Hitachi Regulus SU8100). UV-vis diffuse reflectance spectroscopic measurements were performed with a Hitachi Model UH5700 Spectrophotometer, using BaSO<sub>4</sub> as the reference sample. The functional groups of the samples were characterized by Fourier transform infrared spectroscopy (FT-IR, Thermo Fisher Scientific NICOLET 6700) in the spectral range of 4000 to 400 cm<sup>-1</sup> using KBr particles. Thermogravimetric analysis (TGA) was performed using a NETZSCH STA 449 F5 instrument, with testing conditions ranging from 30 to 600 °C and a temperature change rate of 10 °C min<sup>-1</sup>.

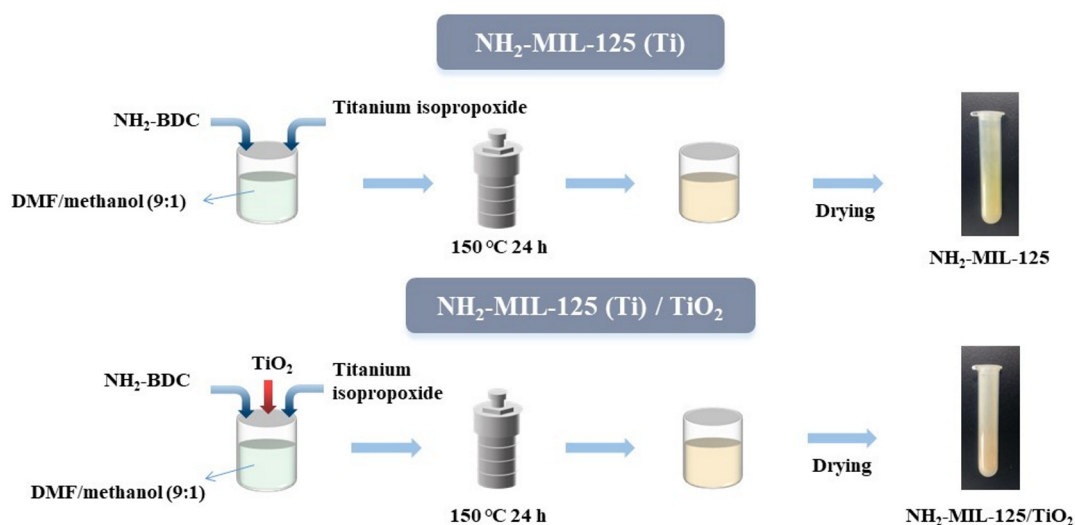


Fig. 1. Scheme for the synthesis of MOF and composites MOF/TiO<sub>2</sub>.

#### 2.4 Photocatalytic degradation of pesticides

The photocatalytic degradation experiments were carried out in a double-layer quartz vessel (250 mL in volume) that could be filled with cooling water, and the reactor temperature (20 °C) was controlled with flowing cooling water, using a 300-watt xenon lamp (Beijing Perfect Light PLS-SXE300E) as the light source. A typical neonicotinoid insecticide imidacloprid was selected as the target pollutant to evaluate the photocatalytic performance of the prepared materials. During the experiment, 50 mg of catalyst and 50 mL of an aqueous solution of imidacloprid (initial concentration of 5 mg/L) were simultaneously added into the reactor. First, the mixed solution was stirred under dark conditions for 1 h to reach the adsorption resolution equilibrium. The light source was then activated to initiate and maintain the photocatalytic reaction for 80 minutes. During this time, 1 ml of the sample solution was extracted at regular intervals using a syringe and subsequently filtered through a polyester sulfone filter membrane with a layer thickness of 0.22 μm. A high-performance liquid chromatograph (HPLC, Agilent 1100 series) equipped with a C18 column and a DAD detector was used to determine the concentration of IMD in the samples. The flow rate of the mobile phase was 1.0 mL/min, methanol/water (50:50 v/v), the detection wavelength was 270 nm, and the injection volume was 10 μL.

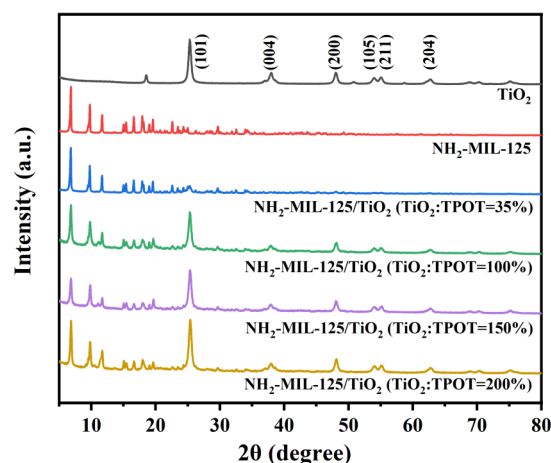


Fig. 2. XRD patterns of TiO<sub>2</sub>, NH<sub>2</sub>-MIL-125, NH<sub>2</sub>-MIL-125/TiO<sub>2</sub>.

### 3. Results and Discussion

The composite components (TiO<sub>2</sub> and NH<sub>2</sub>-MIL-125) and the NH<sub>2</sub>-MIL-125/TiO<sub>2</sub> composite (with a molar ratio of 0.35:1 for TiO<sub>2</sub> P25 to precursor) were characterized by scanning electron microscopy, diffuse reflection spectrum and IR spectroscopy. All NH<sub>2</sub>-MIL-125/TiO<sub>2</sub> composites were analyzed by XRD and TG methods and their photocatalytic properties towards imidacloprid were determined.

Fig. 2 shows X-ray diffraction (XRD) patterns for TiO<sub>2</sub> and as well as NH<sub>2</sub>-MIL-125/TiO<sub>2</sub> composites. The XRD pattern for TiO<sub>2</sub> is consistent with that of commercial TiO<sub>2</sub> sample P25 and confirms the presence of a predominantly ana-

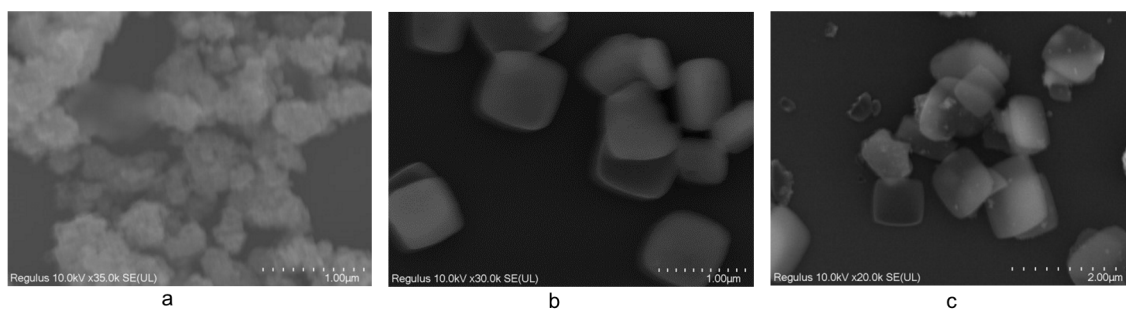


Fig. 3 (a, b, c). SEM images of (a) TiO<sub>2</sub> (P25), (b) NH<sub>2</sub>-MIL-125 (MOF), (c) NH<sub>2</sub>-MIL-125/TiO<sub>2</sub> (composite).

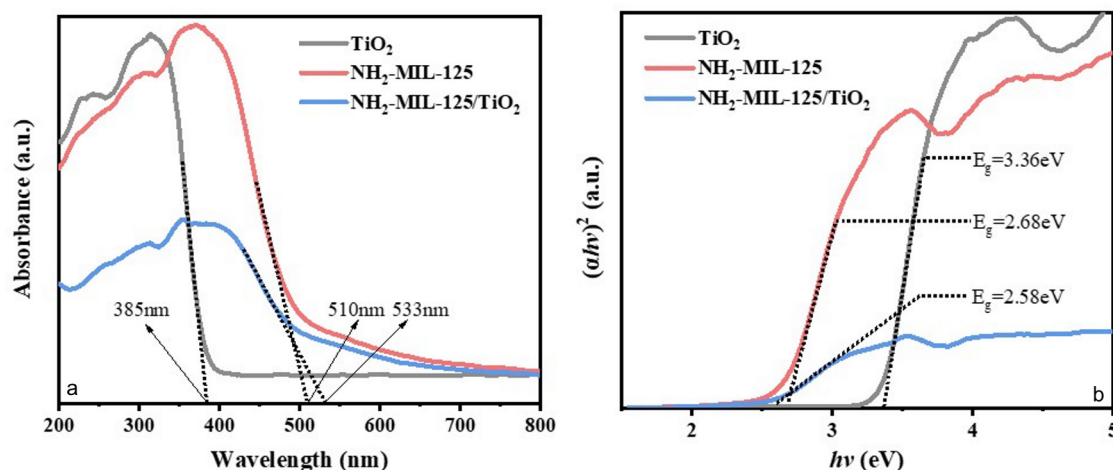


Fig. 4 (a, b). SEM images of (a) TiO<sub>2</sub> (P25), (b) NH<sub>2</sub>-MIL-125 (MOF), (c) NH<sub>2</sub>-MIL-125/TiO<sub>2</sub> (composite).

tase phase [36]. The NH<sub>2</sub>-MIL-125 XRD pattern is consistent with the metal-organic framework structure [37], confirming a successful synthesis, as evidenced by the majority of XRD peaks in the 2θ range of 5 to 25° attributed to it. The XRD pattern of NH<sub>2</sub>-MIL-125/TiO<sub>2</sub> composites exhibited the characteristic peak (101) of TiO<sub>2</sub>, affirming the creation of the composite and the stability of the TiO<sub>2</sub> structure within them. Fig. 2 shows that increasing the ratio of TiO<sub>2</sub> to TPOT results in a higher intensity of the TiO<sub>2</sub> main peak (101).

SEM images confirm the formation of the MOF structure and NH<sub>2</sub>-MIL-125/TiO<sub>2</sub> composites (Fig. 3). The commercial P25 sample exhibits a characteristic structure consisting of small particles up to 100 nm in size that form agglomerates and aggregates [36]. On the other hand, the NH<sub>2</sub>-MIL-125 sample has a typical MOF structure, and particle size ranges mainly up to 500 nm. The NH<sub>2</sub>-MIL-125/TiO<sub>2</sub> composite has a MOF structure with titanium oxide particles distributed on the surface of the material.

It is known that the synthesis method and type of precursors significantly affect the structure and properties of titanium oxide [38]; the band gap is important for photocatalytic ap-

plications. Fig. 4a shows the reflectance spectra for TiO<sub>2</sub>, NH<sub>2</sub>-MIL-125, and NH<sub>2</sub>-MIL-125/TiO<sub>2</sub> samples. Also, Fig. 4b shows the Tauc-plot transformation curve for the corresponding spectra.

As can be seen from Fig. 4a, the diffuse reflectance-absorption spectrum for titanium oxide has a typical appearance and shows the onset of absorption at 385 nm, which is almost identical to the theoretical data [39]. The spectrum for the NH<sub>2</sub>-MIL-125 sample is interesting from the point of view of possible prospects in photocatalytic processes under visible light, since the wavelength at which the absorption starts is at 510 nm (this agrees with the data of other authors [37]) and the absorption is the most intense among the presented samples. The NH<sub>2</sub>-MIL-125/TiO<sub>2</sub> composite is characterized by an even longer absorption wavelength, indicating the probable photocatalytic activity of this composite under visible light. However, the absorption intensity of the composite is low, which may indicate that it generates fewer electron-hole pairs. In Fig. 4b, the band gap of TiO<sub>2</sub> is approximately 3.36 eV, the band gap of NH<sub>2</sub>-MIL-125 is approximately 2.68 eV, and the band gap of the NH<sub>2</sub>-MIL-125/TiO<sub>2</sub> composite material is about 2.58 eV.

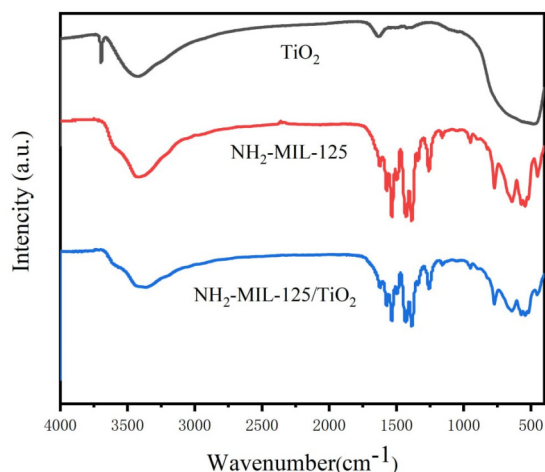


Fig. 5. IR spectra of TiO<sub>2</sub>, NH<sub>2</sub>-MIL-125, NH<sub>2</sub>-MIL-125/TiO<sub>2</sub>.

Fig. 5 shows the IR spectra of TiO<sub>2</sub>, NH<sub>2</sub>-MIL-125, NH<sub>2</sub>-MIL-125/TiO<sub>2</sub> samples. The IR spectrum of the TiO<sub>2</sub> P25 sample is typical for titanium oxide [40]. The broadened peak in the region of 480–600 cm<sup>-1</sup> indicates the presence of both anatase and rutile phases, which is confirmed by the literature.

Signals characteristic of MIL-125-NH<sub>2</sub> are observed at 1530 cm<sup>-1</sup> (N-H stretching), 1420 cm<sup>-1</sup> (CN vibrations), 1570 cm<sup>-1</sup> and 1500 cm<sup>-1</sup> (asymmetric -COO vibrations), and 1390 cm<sup>-1</sup> (symmetric -COO vibrations) [41]. As can be seen from the spectrum of the NH<sub>2</sub>-MIL-125 sample, the bands of the R-COOH functional groups of the starting ligands underwent significant shifts as a result of complexation with Ti (IV). At the same time, we observed the disappearance of the carbonyl group (C=O) band (at 1690 cm<sup>-1</sup>) and the formation of two new bands at 1600–1500 cm<sup>-1</sup> and 1450–1350 cm<sup>-1</sup> corresponding to the asymmetric and symmetric stretching of the carboxylate group (COO<sup>-</sup>), respectively [41]. Thus, the interaction of Ti (IV) with -COOH functional group of the ligands induces the resonant structure of the carboxylate group (-COO). This indicates the complexation and formation of titanium MOFs.

The infrared spectrum of the NH<sub>2</sub>-MIL-125/TiO<sub>2</sub> composite corresponds to that of the MIL-125-NH<sub>2</sub> sample. This may indicate that this sample contains a small amount of titanium oxide in the composite. Based on the data obtained, further studies were conducted on the thermal analysis of the samples.

The thermal analysis data confirms that the NH<sub>2</sub>-MIL-125/TiO<sub>2</sub> composite sample with a molar ratio of 0.35:1 for TiO<sub>2</sub> P25 to TPOT

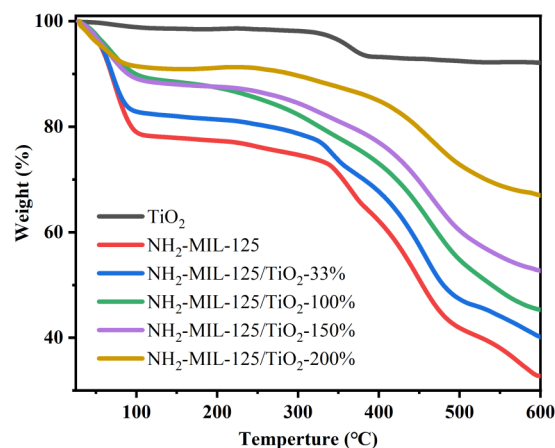


Fig. 6. TG analysis of TiO<sub>2</sub>, NH<sub>2</sub>-MIL-125, NH<sub>2</sub>-MIL-125/TiO<sub>2</sub>.

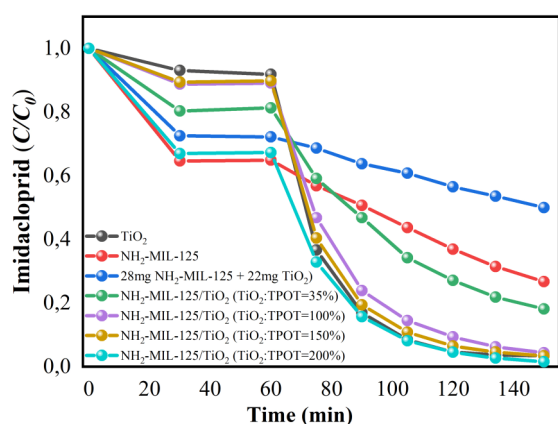


Fig. 7. Disintegration kinetics curves of imidacloprid.

precursor contains no more than 30% wt. of titanium oxide (Fig. 6). In addition, we have analyzed composite samples with higher titanium oxide content with the following P25 to TPOT precursor ratios: 1:1, 1.5:1, and 2:1. As can be seen from Fig. 6, the NH<sub>2</sub>-MIL-125/TiO<sub>2</sub> samples contain ~40, 50 and 63% wt. titanium oxide accordingly.

Fig. 7 shows the kinetic dependences of imidacloprid degradation in aqueous solutions. As can be seen from Fig. 7, a minor degree of imidacloprid degradation is observed within up to 60 minutes, which is associated with the adsorption process. After turning on the ultraviolet light, the degree of pesticide degradation in all cases increased significantly.

Further progression of the photocatalytic process leads to even more intensive decomposition of the pesticide under study, which after 80 minutes of irradiation is almost 100%. It should be noted that the activity of the photocatalysts differs slightly from the adsorption

capacity of the catalysts. It can be seen that samples NH<sub>2</sub>-MIL-125 and NH<sub>2</sub>-MIL-125/TiO<sub>2</sub> (2:1) exhibit higher adsorption capacity, while samples NH<sub>2</sub>-MIL-125/TiO<sub>2</sub> (2:1) and TiO<sub>2</sub> exhibit the most pronounced photocatalytic activity. Thus, the data indicate that the most effective photocatalyst is NH<sub>2</sub>-MIL-125/TiO<sub>2</sub> (2:1) sample, which also shows high adsorption capacity for imidacloprid relative to other photocatalysts. In the future, it is planned to investigate nanocomposites with an even higher content of titanium (IV) oxide and determine their photocatalytic activity to various pesticides.

#### 4. Conclusions

The successful synthesis of NH<sub>2</sub>-MIL-125 MOF and NH<sub>2</sub>-MIL-125/TiO<sub>2</sub> nanocomposites by the solvothermal method was carried out and characterized. X-ray diffraction, electron microscopy, UV, IR and FT-IR spectroscopy and TGA analysis showed that TiO<sub>2</sub> and MOF have typical properties, and the properties of the composite were similar to those of MOF. The found band gap values of MOF and MOF/TiO<sub>2</sub> composite (2.68 eV and 2.58 eV, respectively) indicate their potential promising use in photocatalytic processes in the visible light region. The study of the photocatalytic activity towards imidacloprid indicates a two-step degradation, which is most efficient and reaches almost 100% when using the MOF/TiO<sub>2</sub> composite with the highest titanium (IV) oxide content. In the future, it is planned to increase the content of titanium (IV) oxide and study the effect on various types of pesticides.

#### Acknowledgements.

The authors gratefully acknowledge the National Research Foundation of Ukraine for funding the project (project registration number 2020.02/0024) and the China Scholarship Council for financial support of postgraduate studies in Ukraine.

#### References

1. Mu H, Yang X, Wang K, et al., *Chemosphere*, 326, 138428 (2023). DOI: 10.1016/j.chemosphere.2023.138428.
2. Zhang X, Huang Y, Chen WJ, et al., *Environ. Res.*, 218, 114953 (2023). DOI: 10.1016/j.envres.2022.114953.
3. Mojiri A, Zhou JL, Robinson B, et al., *Chemosphere*, 253, 126646 (2020). DOI: 10.1016/j.chemosphere.2020.126646.
4. Asghar A, Mabarak S, Ashraf B, et al., *Inorg. Chem. Commun.*, 159, 111790 (2024). DOI: 10.1016/j.inoche.2023.111790.
5. Roshani M, Nematollahi D, Ansari A, et al., *Chemosphere*, 346, 140597 (2024). DOI: 10.1016/j.chemosphere.2023.140597.
6. Pirsahab M, Moradi N., *RSC Adv.*, 10, 7396–7423 (2020). DOI: 10.1039/C9RA11025A.
7. GOH PS, Ahmad NA, Wong TW, et al., *Chemosphere*, 307(3), 136018 (2022). DOI: 10.1016/j.chemosphere.2022.136018.
8. Kuzminchuk A, Burmak A, Litynska M, et al., *Appl. Nanosci.*, 13, 5335–5343 (2023). DOI: 10.1007/s13204-023-02792-8.
9. Dontsova T, Kyrii S, Yanushevska O, et al., *Chem. Pap.*, 76, 7667–7683 (2022). DOI: 10.1007/s11696-022-02433-4.
10. Kutuzova A, Dontsova T, Kwapinski W, et al., *Mol. Cryst. Liq. Cryst.*, 751, 28–40 (2022). DOI: 10.1080/15421406.2022.2073526.
11. Ribeiro AR, Nunes OC, Pereira MFR, et al., *Environ. Int.*, 75, 33–51 (2015). DOI: 10.1016/j.envint.2014.10.027.
12. Bartolomeu M, Neves MGPMS, Faustino MAF, et al., *Photochem. Photobiol. Sci.*, 17, 1573–1598 (2020). DOI: 10.1039/C8PP00249E.
13. Varma KS, Tayade RJ, Shah KJ, et al., *Water-Energy Nexus*, 3, 46–61 (2020). DOI: 10.1016/j.wen.2020.03.008.
14. Wei Z, Liu J, Shangguan W., *Chinese J. Catal.*, 41(10), 1440–1450 (2020). DOI: 10.1016/S1872-2067(19)63448-0.
15. Dontsova TA, Kutuzova AS, Bila KO, et al., *J. Nanomater.*, 2020, 8349480 (2020). DOI: 10.1155/2020/8349480.
16. Kutuzova A, Dontsova T, Kwapinski W., *J. Inorg. Organomet. Polym. Mater.*, 30, 3060–3072 (2020). DOI: 10.1007/s10904-020-01467-z.
17. Kutuzova A, Dontsova T., *Proceedings of the 2018 IEEE 8th International Conference Nanomaterials: Application & Properties, 2018 Sep 9–14, Zatoka, Ukraine*, 1–5 (2019). DOI: 10.1109/NAP.2018.8914747.
18. Kutuzova A, Dontsova T., *Proceedings of the 2017 IEEE 7th International Conference Nanomaterials: Application & Properties, 2017 Sep 10–15, Odessa, Ukraine*, 01NNPT02–1-01NNPT02-5 (2017). DOI: 10.1109/NAP.2017.8190182.
19. Fagan R, McCormack DE, Dionysiou DD, et al., *Mater. Sci. Semicond. Process.*, 42(1), 2–14 (2016). DOI: 10.1016/j.mssp.2015.07.052.
20. Kyrii S, Dontsova T, Kosogina I, et al., *Eastern-European Journal of Enterprise Technologies*, 4(6(112)) 67–74 (2021). DOI: 10.15587/1729-4061.2021.238347.

21. Abdurahman MH, Abdullah AZ, Shoparwe NF., *Chem. Eng. J.*, 413, 127412 (2021). DOI: 10.1016/j.cej.2020.127412.
22. Majumdar A, Pal A., *Clean Technol. Environ. Policy*, 22, 11–42 (2020). DOI: 10.1007/s10098-019-01766-1.
23. Abbasnia A, Zarei A, Yeganeh M, et al., *Inorg. Chem. Commun.*, 145, 109959 (2022). DOI: 10.1016/j.inoche.2022.109959.
24. Batten SR, Neville SM, Turner DR., *Angew. Chem. Int. Ed.*, 48(27), 4890–4891 (2009). DOI: 10.1002/anie.200902588.
25. Jiao L, Seow JYR, Skinner WS, et al., *Mater. Today*, 27, 43–68 (2019). DOI: 10.1016/j.mattod.2018.10.038.
26. Falcaro P, Ricco R, Yazdi A, et al., *Coord. Chem. Rev.*, 307(2), 237–254 (2016). DOI: 10.1016/j.ccr.2015.08.002.
27. Karthik P, Balaraman E, Neppolian B., *Catal. Sci. Technol.*, 8, 3286–3294 (2018). DOI: 10.1039/C8CY00604K.
28. Horiuchi Y, Toyao T, Saito M, et al., *J. Phys. Chem. C.*, 116(39), 20848–20853 (2012). DOI: 10.1021/jp3046005.
29. Slater AG, Cooper AI., *Science*, 348(6238) (2015). DOI: 10.1126/science.aaa8075.
30. Forster PM, Thomas PM, Cheetham AK., *Chem. Mater.*, 14(1), 17–20 (2002). DOI: 10.1021/cm010820q.
31. George P, Dhabarde NR, Chowdhury P., *Mater. Lett.*, 186, 151–154 (2017). DOI: 10.1016/j.matlet.2016.09.099.
32. Devic T, Serre C., *Chem. Soc. Rev.*, 43, 6097–6115 (2014). DOI: 10.1039/C4CS00081A.
33. Dong J, Cui P, Shi PF, et al., *J. Am. Chem. Soc.*, 137(51), 15988–15991 (2015). DOI: 10.1021/jacs.5b10000.
34. Low JJ, Benin AI, Jakubczak P, et al., *J. Am. Chem. Soc.*, 131(43), 15834–15842 (2009). DOI: 10.1021/ja9061344.
35. Wang H, Yuan X, Wu Y, et al., *J. Hazard. Mater.*, 286, 187–194 (2015). DOI: 10.1016/j.jhazmat.2014.11.039.
36. González-Burciaga LA, Núñez-Núñez CM, Morones-Esquivel MM, et al., *Catalysts*, 10(1), 118 (2020). DOI: 10.3390/catal10010118.
37. Yoon JW, Kim DH, Kim JH, et al., *Appl. Catal. B: Environ.*, 244, 511–518 (2019). DOI: 10.1016/j.apcatb.2018.11.057.
38. Dontsova T, Ivanenko I, Astrelin I., *Springer Proceedings in Physics: Nanoplasmonics, Nano-Optics, Nanocomposites, and Surface Studies*, 167, 275–293 (2015). DOI: 10.1007/978-3-319-18543-9\_19.
39. Fidalgo A, Letichevsky S, Santos BF., *J. Photochem. Photobiol. A*, 405, 112870 (2021). DOI: 10.1016/j.jphotochem.2020.112870.
40. Al-Amin M, Dey S, Rashid T, et al., *International Journal of Latest Research in Engineering and Technology*, 2, 14–21 (2016).
41. Castellanos NJ, Rojas ZM, Camargo HA, et al., *Transit. Met. Chem.*, 44, 77–87 (2019). DOI: 10.1007/s11243-018-0271-z.